Cell Reports

Supplemental Information

Membrane charge directs the outcome of F-BAR domain lipid binding and autoregulation

Charlotte F. Kelley, Emily M. Messelaar, Tania L. Eskin, Shiyu Wang, Kangkang Song, Kalanit Vishnia, Agata N. Becalska, Oleg Shupliakov, Michael F. Hagan, Dganit Danino, Olga S. Sokolova, Daniela Nicastro, Avital A. Rodal

Supplemental Data

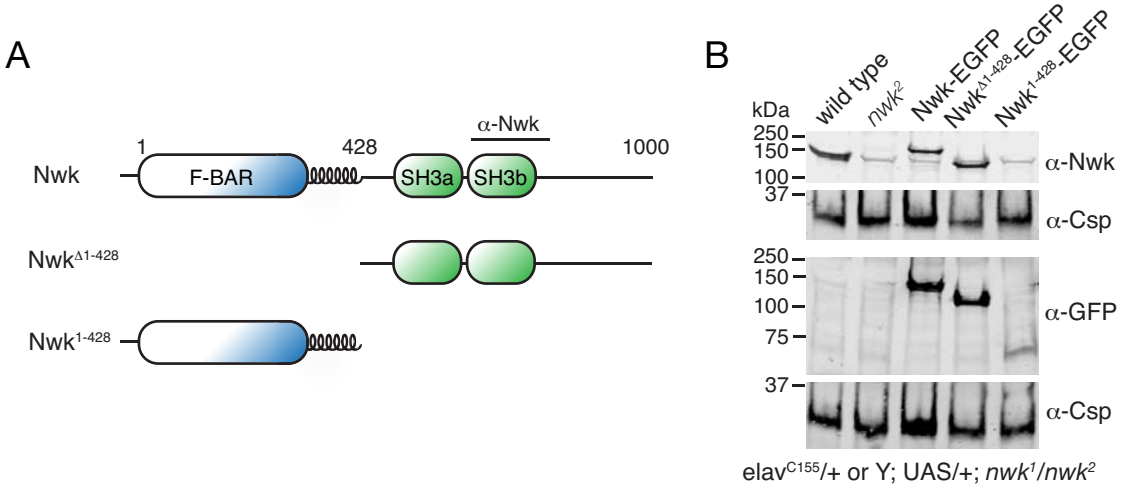

Figure S1 (associated with Figure 1). Expression level of Nwk-EGFP constructs compared to endogenous Nwk in adult head extracts.

(A) Schematic of Nwk constructs expressed in a wild type or *nwk* mutant background

(B) Immunoblot of Nwk construct expression levels in adult head extracts.

A

```
Nwk-SH3b          639 EWCIALYDYDATAEDELTFEEGDKIKIITKT 669
FCHSD1-SH3b       547 FLARALYSYTGQSEEELSFPEGALIRLLPRA 577
FCHSD2-SH3b       570 CFVKALYDYEGQTDDELSFPEGAIIRILNKE 600
Syndapin 1-SH3    385 VRVRALYDYDGQEQDELSFKAGDELTKL--- 412
Nwk-SH3a          546 FKCTALYSYTAQNPDELTIVENEQLEVV--- 573
FCHSD1-SH3a       469 CPAHVVFGYQAGREDELTITEGEWLEVI--- 497
FCHSD2-SH3a       472 LTCKVVYSYKASQPDELTIEEHEVLEVI--- 499
                          .:: * .   :**::     :  :

Nwk-SH3b          670 AHGVDDGWWEGEL-DGKFGNFPSLVVEECD  698
FCHSD1-SH3b       578 QDGVDDGFWRGEF-GGHVGVFPSLLVEELL  606
FCHSD2-SH3b       601 -NQDDDGFWEGEF-SGRIGVFPSVLVEELS  628
Syndapin 1-SH3    413 GEEDEQGWCRGRLDSGQLGLYPANYVEAI-  441
Nwk-SH3a          574 GEGDGDGWLRARNYRGEEGYVPHNYLDIDQ  603
FCHSD1-SH3a       498 EEGDADEWVKARNQHGEAGFVPERYLNFPD  526
FCHSD2-SH3a       500 EDGDMEDWVKARNKVGQVGYVPEKYLQFPT  529
                        .   : : ...   *. *  *   ::
```

B

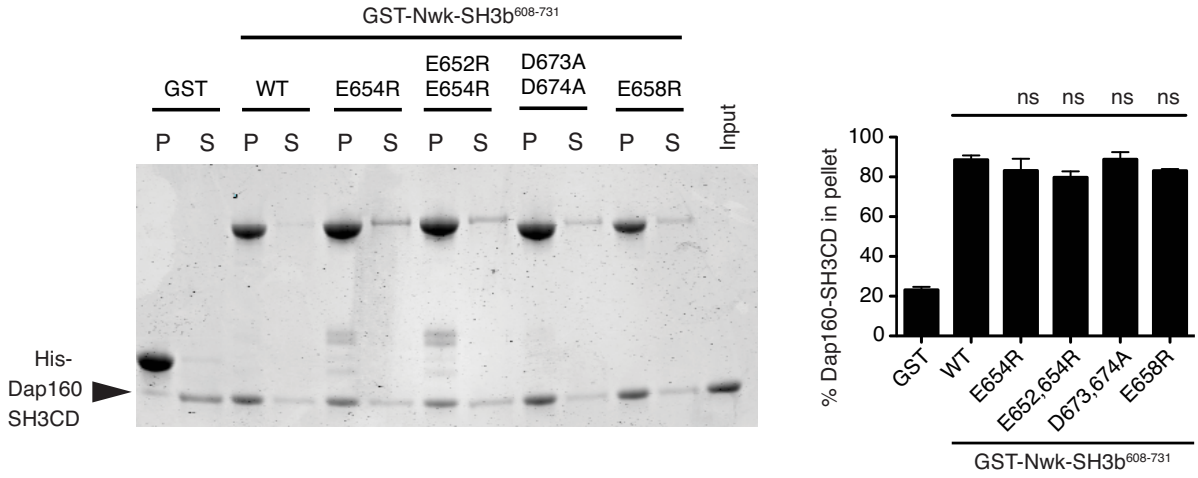

Figure S2 (associated with Figure 3).

(A) Alignment of Nwk SH3 domain with Syndapin 1 and mammalian homologues FCHSD1 and FCHSD2.

(B) Co-sedimentation of 6xHis-Xpress-Dap160SH3CD (3.75 μM) with GST-Nwk-SH3b variants (125 ng/μL; 3 μM). Image shows representative Coomassie-stained gel, with quantification of average ± s.e.m from three independent reactions.

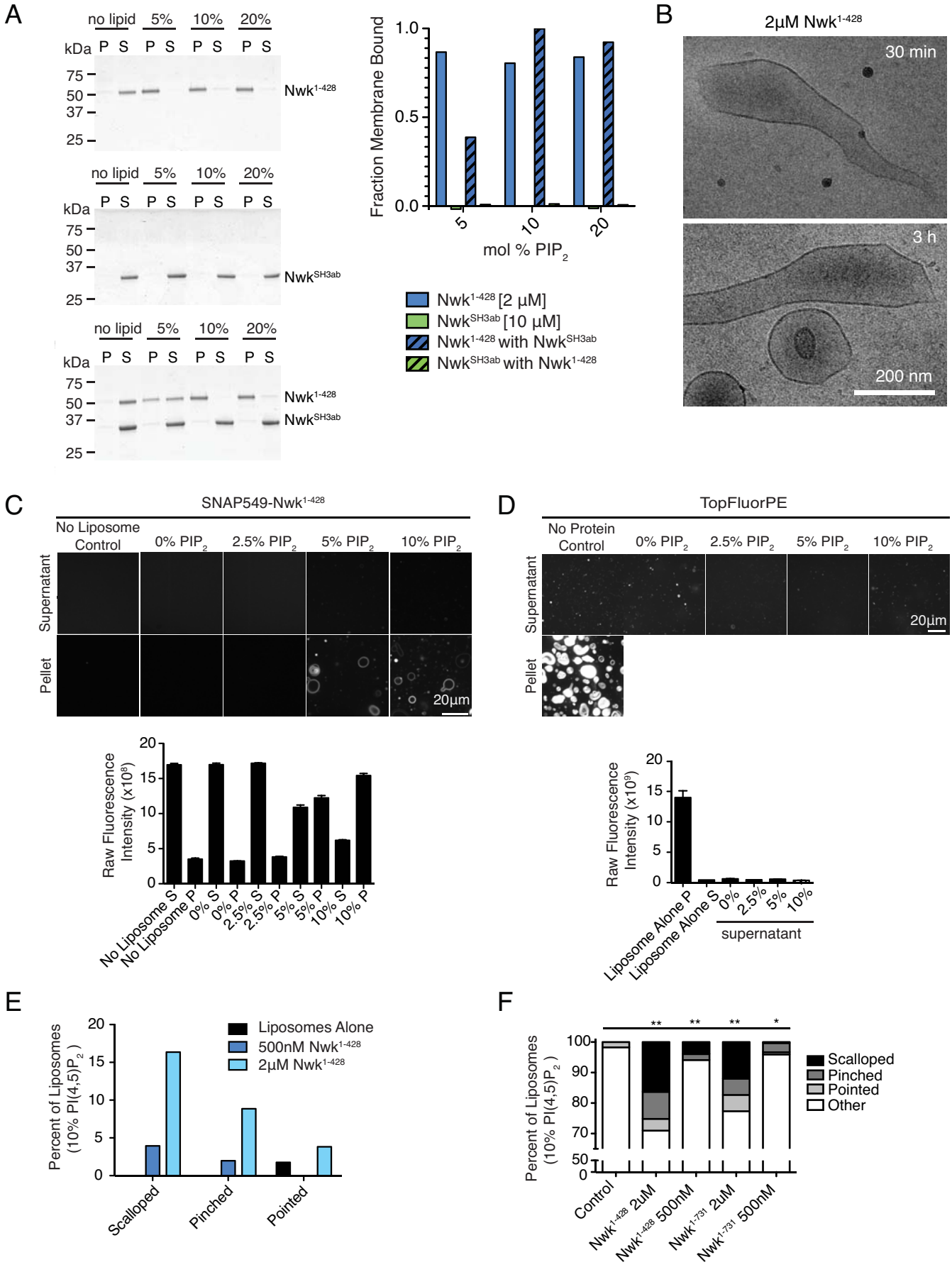
A
no lipid
5%
10%
20%
kDa
P S P S P S P S
75
50
37
25
Nwk1-428
NwkSH3ab
Fraction Membrane Bound
1.0
0.5
0.0
5
10
20
mol % PIP2
Nwk1-428 [2 μM]
NwkSH3ab [10 μM]
Nwk1-428 with NwkSH3ab
NwkSH3ab with Nwk1-428
B
2μM Nwk1-428
30 min
3 h
200 nm
C
SNAP549-Nwk1-428
No Liposome Control
0% PIP2
2.5% PIP2
5% PIP2
10% PIP2
Supernatant
Pellet
20μm
Raw Fluorescence Intensity (x10⁸)
No Liposome S
No Liposome P
0% S
0% P
2.5% S
2.5% P
5% S
5% P
10% S
10% P
D
TopFluorPE
No Protein Control
0% PIP2
2.5% PIP2
5% PIP2
10% PIP2
Supernatant
Pellet
20μm
Raw Fluorescence Intensity (x10⁹)
Liposome Alone P
Liposome Alone S
0%
2.5%
5%
10%
supernatant
E
Percent of Liposomes (10% PI(4,5)P2)
Liposomes Alone
500nM Nwk1-428
2μM Nwk1-428
Scalloped
Pinched
Pointed
F
Percent of Liposomes (10% PI(4,5)P2)
**
**
**
*
Scalloped
Pinched
Pointed
Other
Control
Nwk1-428 2uM
Nwk1-428 500nM
Nwk1-731 2uM
Nwk1-731 500nM

Figure S3 (associated with Figure 4).

(A) Purified proteins (10 μM $Nwk^{536-731}$; 2 μM Nwk^{1-428}) were incubated with liposomes containing 80-X% PC, 15% PE, 5% PS and X% $PI(4,5)P_2$ (where X is the concentration indicated on the graph) and subjected to liposome cosedimentation assays. Images show representative Coomassie staining of supernatant (S) and pellet (P) fractions of controls with no added liposomes, and samples incubated with 5,10 and 20% $PI(4,5)P_2$ liposomes. Graph shows quantification of percent membrane bound protein from the Coomassie stained gels.

(B) Cryo-EM of liposomes incubated with Nwk^{1-428} for 30 min or 3 h. At longer incubation times, Nwk^{1-428} continues to induce membrane scalloping, pointing, and pinching of 0.27 mM (0.22 mg/ml) [DOPC:DOPE:DOPS:$PI(4,5)P_2$] = 70:15:5:10 liposomes. Scale bar is 200 nm.

(C) Images of pellet and supernatant samples after liposome cosedimentation with 1 μM SNAP549-Nwk^{1-428} +/- liposomes of 80-X% PC, 15% PE, 5% PS and X% $PI(4,5)P_2$ with indicated amounts of $PI(4,5)P_2$. Quantification of mean raw fluorescence intensity of SNAP549 for each sample ± s.e.m. from at least 10 full field-of-view images.

(D) Images of supernatant samples and control pellet sample of TopFluor-PIP_2-labeled liposomes after cosedimentation with +/- 1 μM Nwk^{1-428} of 80-X% PC, 14.9% PE, 5% PS, 0.1% TopFluorPE, and X% $PI(4,5)P_2$ with indicated amounts of $PI(4,5)P_2$. Quantification of mean raw fluorescence intensity of TopFluorPIP_2 for each sample ± s.e.m. from at least 10 full field-of-view images.

(E) Characterization of liposome morphology from cryo-EM of liposomes alone compared to liposomes incubated with 500nM or 2 μM Nwk^{1-428}. Liposome composition was 0.30 mM (0.24 mg/ml) [DOPC:DOPE:DOPS:$PI(4,5)P_2$] = 70:15:5:10. (F) Distribution of vesicle morphology was dependent on Nwk. Vesicle morphologies after incubation with Nwk^{1-428} or Nwk^{1-731} are significantly different from control vesicles. χ^2 *p<0.05, **p<0.005.

Condition compared to control	X^2	d.f.	p-value
2μM Nwk^{1-428}	78.7	3	<.005
500nM Nwk^{1-428}	23.56	3	<.005
2μM Nwk^{1-731}	63.49	3	<.005
500nM Nwk^{1-731}	8.76	3	<.05

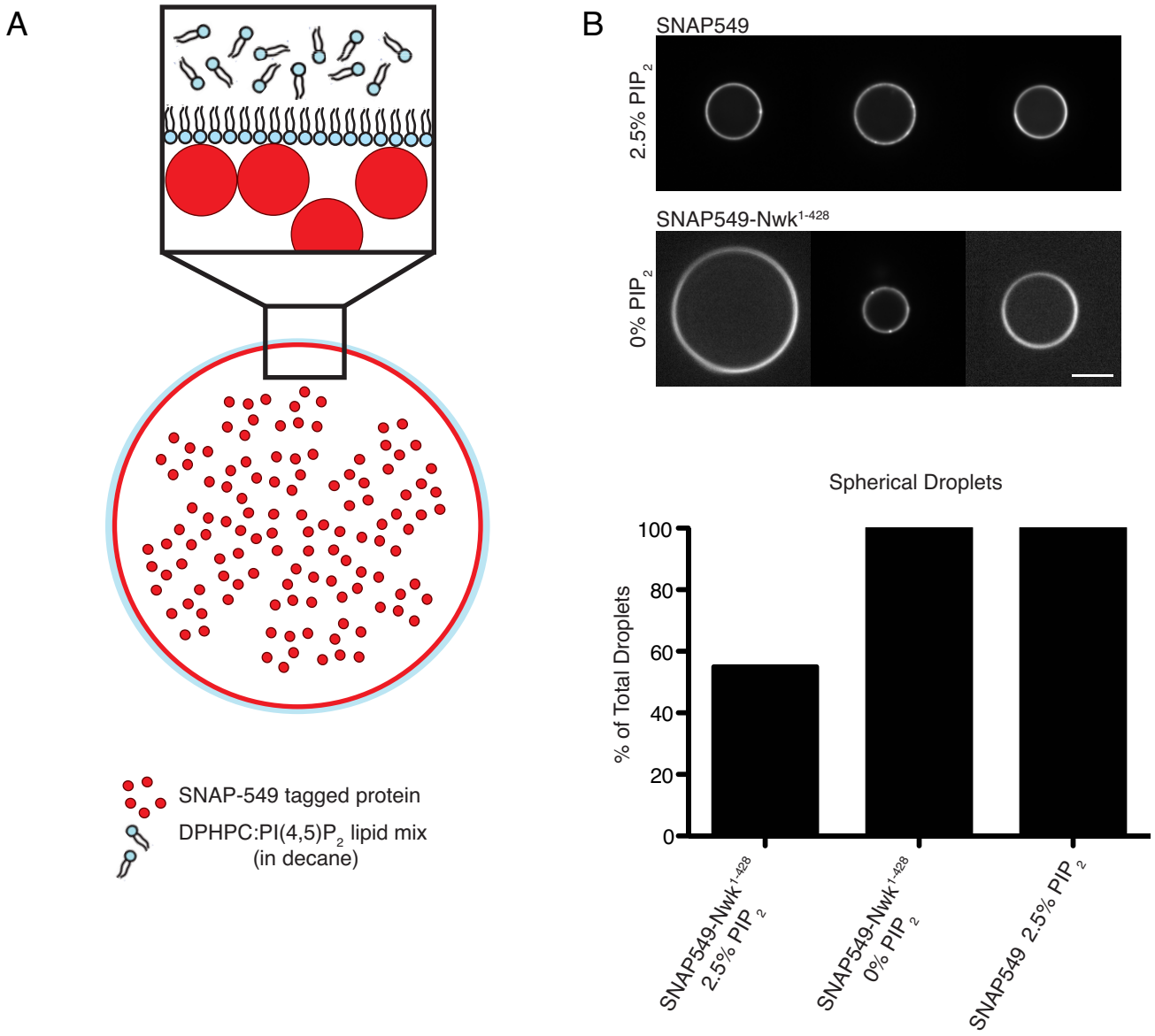

Figure S4 (associated with Figure 6).

(A) Schematic of droplet assay. Droplets were produced by mixing aqueous protein and 20 mg/mL lipid in decane in a 1:50 ratio, creating a water-in-oil emulsion, which formed droplets containing the soluble protein, as in diagram.

(B) Representative images of droplets of 97.5% DPHPC, 2.5% PI(4,5)P2 incubated with 1 μM purified SNAP-549 and 100% DPHPC incubated with 1 μM SNAP549-Nwk$^{1-428}$, imaged after 1 hour. Scale bar is 10 μm. Quantification is shown of the percent of total control droplets that remained spherical after 1 hour compared to 2.5% PI(4,5)P2-surrounded droplets incubated with Nwk$^{1-428}$.

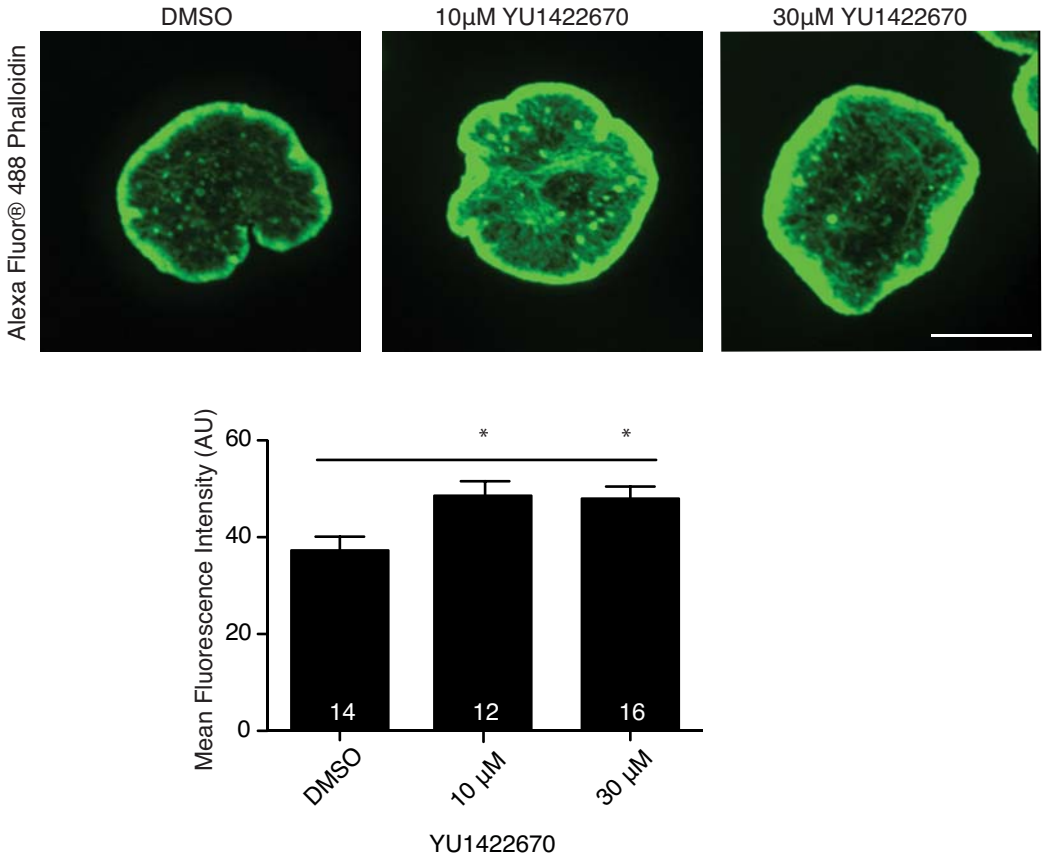

Figure S5 (associated with Figure 7).

The OCRL inhibitor YU1422670 increases F-actin levels in *Drosophila* S2 cells. Images show Alexa Fluor® 488 Phalloidin staining of maximum intensity z-projections. Cells treated with YU1422670 have a significantly higher mean fluorescence intensity compared to DMSO-treated control cells. Scale bar is 10 µM.

Table S1

Orientation	Degree of rotation	Nwk^{1-428} 2.5% PIP2				Nwk^{1-428} 10% PIP2		
		grid A	grid B	grid C	grid D	grid A	grid B	grid C
Convex down	0			22				62
	10	97	29	76				86
	20		15	84	24		63	
	30	130		58	33	185	12	49
	40	152	22	65	66	94	22	
	50	64	60			258	69	59
	# particles	443	126	305	123	537	166	256
	fraction particles	0.34	0.25	0.37	0.35	0.41	0.36	0.36
Side down	60	144	14		41	114		35
	70	38	30	46	28		24	85
	80	73	27	27		42	13	
	90	56		40			30	
	100	40	50	47		59	50	35
	110		16	24		52	37	
	120			23		176		158
	# particles	351	137	207	69	443	154	313
	fraction particles	0.27	0.27	0.25	0.20	0.33	0.34	0.43
Concave down	130	48	89	56	24	44	10	12
	140	34	29	78	109	180		35
	150	236	72	31	22	70	59	74
	160	61	37	85		49	29	30
	170			31				
	180	115	12	22			38	
	# particles	494	239	303	155	343	136	151
	fraction particles	0.38	0.48	0.37	0.45	0.26	0.30	0.21
R range		0.5-0.8	0.7-0.9	0.4-0.7	0.7-0.9	0.6-0.9	0.5-0.75	0.7-0.9
total particles		1288	502	815	347	1323	456	720

Table S1 (associated with Figure 6): Quantification of Nwk^{1-428} orientations on membrane monolayers by EM and single particle analysis, corresponding to **Figure 6F**. Data sets represent independently prepared EM grids. Particles were sorted into class averages and compared to 2D projections of the predicted Nwk structure rotated around its long axis in 10º increments, and filtered to 20 Å. Class averages were assigned to the orientation with the highest correlation coefficient (R). R value ranges for each data set are shown.

Supplemental Movie Legends

Movies 1-3 (associated with Figure 5). Time-lapse images from the GUV FRAP assay (Fig. 5). NBD-PE-labeled GUVs were incubated with 500 nM SNAP-549-tagged Nwk variants and imaged by spinning disk confocal microscopy. Lipid composition was DOPC:POPE:DOPS:PI(4,5)P_2:NBD-PE = 75:14.5:5:5:.5. Scale bar is 10μm. Movies show a timelapse of Nwk-bound vesicles over 10 minutes. A small area of the membrane is bleached at 10 sec. **Movie 1** shows a Nwk^{1-731}-bound vesicle that is deformed and does not recover protein fluorescence. **Movie 2** shows a spherical Nwk^{1-428}-bound vesicle, which recovers protein fluorescence very rapidly after photobleaching. **Movie 3** shows a deformed Nwk^{1-428}-bound GUV, which does not recover protein fluorescence. Insets in the first frame show NBD-PE signal, depicting membrane morphology pre-bleach. Time-lapse images were taken at 2 sec intervals and are shown at 10 frames/s (20x real-time).

Movies 4-5 (associated with Figure 6). Time-lapse images of droplets being actively deformed by Nwk. Droplets encapsulated by 97.5%DPHPC, 2.5%PI(4,5)P_2 were incubated with 1 μM purified SNAP549-Nwk^{1-428} (**Movie 4**) or Nwk^{1-731}(**Movie 5**). Time-lapse images were taken at 2.5 sec intervals and are shown at 10 frames/s (25x real-time).

Supplemental Experimental Procedures

Fly stocks, larval immunohistochemistry and NMJ morphology analysis

Flies were cultured using standard media and techniques. UAS-Nwk constructs were generated using Gateway technology (Invitrogen, Inc.) in pBI-UASC-EGFP (Wang et al., 2011). These transgenes were injected into flies (Genetic Services Inc. Cambridge, MA), using Φc381 recombinase at the Attp40 locus (Ni et al., 2008), to ensure that all constructs were in a similar genomic context. For rescue experiments, transgenes were crossed into the nwk^{2} mutant background, and then crossed to $elav^{C155}$; nwk^{1} (Coyle et al., 2004). Immunoblots were conducted on lysates from adult heads, using α-Nwk (Coyle et al., 2004), α-GFP (598, MBL International, Woburn, MA), and α-Csp (6D6, (Zinsmaier et al., 1994)) antibodies and imaged using a LICOR Odyssey device.

For analysis of NMJ morphology and protein localization, flies were cultured at low density at 25ºC. Wandering 3rd instar larvae were dissected in calcium-free HL3.1 saline (Feng et al., 2004) and fixed for 30 min in HL3.1 containing 4% formaldehyde before antibody staining. NMJs on muscle 6/7, segment A3 and muscle 4, segments A2 and A3 were selected for analysis of NMJ morphology, and imaged at room temperature on an Evos FL epifluorescence microscope (Life Technologies, Grand Island, NY) using a 20x objective (n.a. 0.45). Representative confocal images were captured with a 63x objective (n.a. 1.4) on a Marianas spinning disk confocal system (see below). NMJs were stained with α-Cpx and Alexa 488-conjugated secondary antibodies (Huntwork and Littleton, 2007) and α-Dlg and Rhodamine Red-X-conjugated secondary antibodies (Parnas et al., 2001). Both type 1b and type 1s boutons were quantified on muscle 6/7. Only type Ib innervation, delineated by extensive postsynaptic α-Dlg staining, was quantified on muscle 4. Satellite boutons were defined as strings of five or fewer boutons extending from the main axis of the NMJ. For localization studies, larval fillets were fixed as above and labeled with α-BRP and Rhodamine Red-X-conjugated secondary antibodies and Alexa-647-α-HRP (Jackson Immunoresearch, West Grove, PA).

Light microscopy

Confocal imaging of GUVs, cell-sized water droplets, liposomes, S2 cells, and larval salivary glands was conducted at room temperature on a Marianas spinning disk

confocal system (3I, Inc, Denver,CO), consisting of a Zeiss Observer Z1 microscope equipped with a Yokagawa CSU-X1 spinning disk confocal head, a QuantEM 512SC EMCCD camera, PLAN APOCHROMAT 63X or 100x oil immersion objectives (n.a. 1.4), a Photonics Instruments Micropoint photo-ablation device, and Slidebook software. Confocal imaging of larval CNS and NMJ was conducted at room temperature on a Nikon Ni-E upright microscope, equipped with a 100X (n.a. 1.45) oil immersion objective, a Yokogawa CSU-W1 spinning disk head, and an Andor iXon 897U EMCCD camera. Images were collected using Nikon Elements AR software. Fluorescence microscopy image analysis was performed in Image J. For S2 cell protrusion quantification, perimeter and area were calculated from maximum intensity projection images of confocal stacks of at least 9 cells per sample.

Cell culture

S2 cells were cultured, transfected with Effectene, spread for 1 h on Concanavalin-A-coated coverslips, and imaged on a spinning disk confocal microscope (see above) as described previously (Becalska et al., 2013). GFP-tagged expression constructs were generated using Gateway technology as described (Becalska et al., 2013).

For the OCRL inhibitor experiment, cells were incubated with 1% by DMSO control or YU1422670 for 15 minutes before spreading for 1 hour on Concanavalin-A-coated coverslips. Cells were then fixed for 30 minutes in 4% formaldehyde in PBS with 0.1% Triton-X100 and stained with rhodamine phalloidin (Molecular Probes, 1:200) and mounted in Mowiol with DABCO before imaging on a spinning disk confocal microscope (see above) as described previously (Becalska et al., 2013).

Protein alignments, purification, and interaction assays

Protein sequences were aligned using ClustalW2 (Larkin et al., 2007). A homology model of the Nwk SH3b domain was constructed using the Protein Homology/Analogy Recognition Engine (PHYRE), version 2.0 (www.sbg.bio.ic.ac.uk/phyre/). Structural depictions were created using MacPyMOL 2.0.

BL21 DE3 cells transformed with the indicated constructs were grown to log phase and induced with 0.4 M IPTG at room temperature overnight. N-terminally His-

Xpress-tagged and His-Xpress-SNAP-tagged proteins were purified essentially as previously described (Becalska et al., 2013). GST fusions were purified from extracts with glutathione agarose (Thermo Scientific, Waltham MA) in 20 mM Tris 7.5, 20 mM KCl, and 0.5 mM dithiothreitol (DTT) supplemented with protease inhibitors (P2714 (Sigma-Aldrich, St. Louis, MO) and 0.5 mg/mL pepstatin A). Beads were aliquoted, flash frozen in liquid N_2, and stored at -80^{o}C. For pull-down assays, concentrations of GST fusions on beads were normalized using empty beads and bead volume was restricted to two-thirds of the total volume for all reactions. GST fusions were incubated with agitation with His-tagged target proteins at room temperature for one hour in binding buffer (20 mM Tris pH 8.0, 20 mM KCl, 0.5 mM DTT). For salt sensitivity experiments, the indicated concentrations of NaCl were used in place of KCl in the binding buffer. Beads were then pelleted and washed once with buffer after removing the supernatant. Pellets and supernatants were then boiled in Laemmli Sample Buffer and fractionated by SDS-PAGE, followed by Coomassie staining or immunoblotting.

Lipid interaction assays, GUVs, and water droplets

Lipid cosedimentation assays were conducted as previously described (Becalska et al., 2013). Liposomes were swelled from dried lipid films in 20 mM HEPES, pH 7.5 and 100 mM NaCl. Proteins were then mixed with 1 mg/ml liposomes, incubated for 30 min at room temperature, and pelleted for 20 min at 18,000g at 4ºC. Pellets and supernatants were then boiled in Laemmli Sample Buffer and fractionated by SDS-PAGE, followed by Coomassie staining. For quantification, the percent of protein in the pellet of protein-alone control samples was subtracted from all experimental samples.

GUVs were generated by electroswelling lipid mixtures on indium titanium oxide (ITO)–coated slides in a Vesicle Prep Pro device (Nanion Technologies, Munich, Germany), as previously described (Becalska et al., 2013). Briefly, 10 µl of 10 mg/ml lipids (composition indicated in Figures and Figure legends) dissolved in 19:1 chloroform:methanol was dried on ITO slides under vacuum, then swelled in 280 µl of 5 mM HEPES and 300 mM sucrose, pH 7.5, for 2 h at 37oC using a 3-V sinusoidal current at 8 Hz.

Imaging of GUVs was performed on a Marianas spinning disk confocal system

(see above). Three microliters of GUVs were diluted into 5 mM HEPES and 150 mM KCl, pH 7.5, incubated with 500 nM SNAP-tagged F-BAR proteins, and imaged using a 100x objective (n.a. 1.4) in multiwell slides (Lab-Tek), precoated with 1 mg/ml BSA. After a 30-minute incubation, 1% agarose in 5 mM HEPES 150 mM KCl, pH 7.5 was added (for a final concentration of 0.5% agarose) to limit GUV mobility. For analysis of fraction of GUVs bound, fields of GUVs were imaged using only the NBD-PE signal. The number of unilamellar GUVs also labeled with SNAP-549-tagged protein was then quantified using Slidebook 6.0 software (3I, Denver, CO). For analysis of GUV morphology, the SNAP-549 signal was used to identify bound vesicles. All non-spherical vesicles were classified as deformed. For FRAP experiments, GUVs were imaged for 10 min at 2 sec intervals, with a pause for bleaching after timepoint 10 (20s) with 75% laser intensity. Prebleach fluorescence was normalized to 1.0 in order to calculate the fraction of fluorescence recovery. Signal intensity over time from a non-bleached region of the GUV was used to correct for photobleaching.

Electron Microscopy

For cryo-EM, liposomes were generated as above, extruded through a 200-nm filter (Avanti Polar Lipids), and incubated with the indicated proteins for 30 min or 3 h. For data shown in **Figs. 4D** and **S3E**, a 4 µl drop of the sample solution was applied to freshly glow-discharged C-flat 1.2/1.3 copper 200 mesh grids (Protochips Inc., Raleigh, NC) and manually plunge-frozen in liquid ethane, and stored in liquid nitrogen until examination. Cryo-specimens were loaded into a Gatan cryoholder and imaged under low-dose conditions using the software SerialEM (Mastronarde, 2005) with a defocus of -2 µm. The micrographs were recorded either using an FEI Tecnai F20 transmission electron microscope (TEM) operated at 200 kV and equipped with a Gatan UltraScan 4000 4k x 4k CCD camera at a nominal magnification of 29,000x, resulting in a pixel size of 3.74 Å, or using an FEI Tecnai F30 TEM operated at 300 kV and equipped with an energy filter (zero-loss filtered with 20eV slit width) and a Gatan 2k x 2k CCD camera at a nominal magnification of 22,500x, resulting in a pixel size of 6.24 Å. For data shown in **Fig. S3B**, samples were treated as described (Danino, 2012). Briefly, a 6 µl drop of the liposome solution was placed on a 400-mesh TEM copper grid covered with a

perforated carbon film (Ted Pella). The drop was manually blotted in the controlled environment vitrification system (CEVS) and the sample was plunged into liquid ethane, and stored in liquid nitrogen until examination. Cryo-specimens were loaded into a cooled Gatan cryo holder and imaged under low-dose conditions using a FEI Tecnai T12 G^2 TEM or a Philips CM120 TEM operated at 120 kV. Images were recorded digitally on Gatan MultiScan 791 camera (CM120) or an Ultrascan 1000 (T12), using DigitalMicrograph software (Gatan, U.K.).

For negative stain electron microscopy and single particle analysis 1 µl of 1 mg/ml lipids (70-X% PC, 15% PE, 10% PS and X% $PI(4,5)P_2$ with <0.1% Rhodamine-PE for visualization) on a 25-µl drop of buffer (20 mM HEPES, pH 7.5, 100 mM NaCl) was incubated in a Teflon well in a humid chamber at 4°C for 1 hr, lifted onto carbon-coated copper EM grids (400 mesh; Ted Pella, Redding, CA), and the buffer was replaced with a solution containing 0.05 or 0.16 µM Nwk^{1-428} for 30 min in a humid chamber at room temperature. The excess liquid was blotted away and samples were negatively stained with 1% uranyl acetate and imaged on a JEOL 2100 TEM operated at 200 kV voltage. Single particle classification and analyses were conducted as previously described (Becalska et al., 2013).

DNA constructs

	Protein	**Vector**	**Reference**
1	Nwk^{1-428}-eGFP	pBI-UASc-EGFP	Becalska *et al*. 2013
2	Nwk^{1-483}-EGFP	pBI-UASc-EGFP	this study
3	Nwk^{1-544}-EGFP	pBI-UASc-EGFP	this study
4	Nwk^{1-607}-EGFP	pBI-UASc-EGFP	this study
5	Nwk^{1-631}-EGFP	pBI-UASc-EGFP	this study
6	Nwk^{1-706}-EGFP	pBI-UASc-EGFP	this study
7	Nwk^{1-731}-EGFP	pBI-UASc-EGFP	this study
8	$Nwk^{1-731(E654R)}$-EGFP	pBI-UASc-EGFP	this study
9	Nwk^{10-731}-EGFP	pBI-UASc-EGFP	this study
10	$Nwk^{429-1000}$-EGFP	pBI-UASc-EGFP	this study
11	Nwk^{1-1000}-EGFP	pBI-UASc-EGFP	this study
12	$FCHSD2^{FL}$-EGFP	pBI-UASc-EGFP	this study
13	$FCHSD2^{1-440}$-EGFP	pBI-UASc-EGFP	this study

14	GST-Nwk$^{608\text{-}731}$	pGEX4t-1	this study
15	GST-Nwk$^{536\text{-}610}$	pGEX4t-1	this study
16	GST-Nwk$^{536\text{-}731}$	pGEX4t-1	this study
17	GST-Nwk$^{608\text{-}731(E652,654R)}$	pGEX4t-1	this study
18	GST-Nwk$^{608\text{-}731(E654R)}$	pGEX4t-1	this study
19	GST-Nwk$^{608\text{-}731(D673,674A)}$	pGEX4t-1	this study
20	His-Nwk$^{1\text{-}428}$	pET-28A	Becalska *et al.* 2013
21	His-Nwk$^{1\text{-}428(\Delta 181\text{-}189\ \text{->NL})}$	pET-28A	Becalska *et al.* 2013
22	His-Nwk$^{1\text{-}633}$	pTrcHisA	this study
23	His-Nwk$^{1\text{-}731}$	pTrcHisA	Rodal *et al.* 2008
24	His-Dap160$^{937\text{-}1097}$	pTrcHisA	this study
25	His-SNAP-Nwk$^{1\text{-}428}$	pET-28A	Becalska *et al.* 2013
26	His-SNAP-Nwk$^{1\text{-}731}$	pET-28A	Becalska *et al.* 2013

Supplemental References

Danino, D. (2012). Cryo-TEM of soft molecular assemblies. Current Opinion in Colloid & Interface Science *17*, 316-329.

Feng, Y., Ueda, A., and Wu, C.F. (2004). A modified minimal hemolymph-like solution, HL3.1, for physiological recordings at the neuromuscular junctions of normal and mutant *Drosophila* larvae. J Neurogenet *18*, 377-402.

Larkin, M.A., Blackshields, G., Brown, N.P., Chenna, R., McGettigan, P.A., McWilliam, H., Valentin, F., Wallace, I.M., Wilm, A., Lopez, R.*, et al.* (2007). Clustal W and Clustal X version 2.0. Bioinformatics *23*, 2947-2948.

Mastronarde, D.N. (2005). Automated electron microscope tomography using robust prediction of specimen movements. J Struct Biol *152*, 36-51.

Zinsmaier, K.E., Eberle, K.K., Buchner, E., Walter, N., and Benzer, S. (1994). Paralysis and early death in cysteine string protein mutants of *Drosophila*. Science *263*, 977-980.